

Remotely Sensed Sea Surface Temperature Variability Off California During a "Santa Ana" Clearing

RONALD J. LYNN

*Southwest Fisheries Center
National Marine Fisheries Service*

JAN SVEJKOVSKY

Scripps Institution of Oceanography

During a prolonged clearing with particularly dry atmospheric conditions over the Southern California Bight, four NOAA 6 satellite overpasses at 12-hour intervals were recorded while a research vessel measured ocean temperatures within the field of view of the satellite. This data set is used to evaluate two versions of an equation for estimating sea surface temperature from satellite data and for examining short-term changes in surface temperature caused by diurnal variation and surface layer movement. Surface temperatures calculated from data taken during a daytime overpass, using two slightly differing versions of a multiwindow atmospheric correction equation, match the ocean temperatures within the expected range of scatter: $\pm 0.6^{\circ}\text{C}$. One version has a mean daytime bias of $+0.5^{\circ}\text{C}$, the other has -0.4°C , and thus the two versions differ by 0.9°C . The satellite-derived sea surface temperatures show a diurnal variation in the range of 0.25° to 1.0°C . Hence the bias of calculated satellite temperatures for the nighttime overpasses differ from those for the daytime; the bias in one version is $+1.2^{\circ}\text{C}$ and in the other is $+0.4^{\circ}\text{C}$. It is suggested that these biases are caused by inherent problems in the selection and matching of satellite and ocean data sets used to determine the equation coefficients as well as poorly understood diurnal variation of the surface temperature as measured by satellite. Advection, evidenced by an image-to-image shift of thermal gradients over 12- and 24-hour periods can produce local temperature changes that add to the problem. Noise in one of the satellite data channels, another part of the problem, is shown to be amenable to filtering techniques. Diurnal differences in satellite-observed surface temperatures are found to vary regionally; larger variation is found in waters that are turbid and have a shallow thermocline. Near surface in situ temperature measurements suggest a diurnal layer variation of 0.2°C , much less than the variation observed by satellite. An estimation of diurnal sea surface temperature variation based on heat budget calculations supports the in situ observations.

INTRODUCTION

The accuracy of sea surface temperature estimation, using infrared (IR) radiometers aboard earth-orbiting spacecraft, is adversely affected by the attenuation of the atmosphere [Maul and Sidran, 1973]. The effect is principally due to varying amounts of water vapor and spatially unresolved clouds, which absorb and reradiate some of the IR radiation emitted from the ocean. As a result, radiometers measure lower brightness temperatures than they would under cloud-free and moisture-free conditions [Barnett *et al.*, 1979; Bernstein, 1982]. Differences of several degrees between radiometer-measured brightness temperatures and in situ sea surface temperatures (SST) are common. A small part of these differences is caused by the existence of a cool "skin" in the upper $10\mu\text{m}$ which is sensed by the satellite radiometer and which is often 0.3°C to 0.6°C less than the in situ SST commonly measured at a depth of 1 m or so [Paulson and Simpson, 1981]. While several techniques have been developed to reduce the effects of atmospheric attenuation, it was only with the deployment of the Advanced Very High Resolution Radiometer (AVHRR) aboard the NOAA 6 and NOAA 7 polar-orbiting meteorological satellites that the means were

provided to effectively accomplish it. The improvements in the AVHRR instrument over its predecessors include lower background noise in the data and the availability of multiple atmospheric-window channels in the IR bands.

Recently published algorithms that provide estimates of SST from IR brightness temperature [Bernstein, 1982; McClain, 1981; McClain *et al.*, 1983] utilize the advanced capabilities of the AVHRR. The algorithms provide for the selection of cloud-free data and the calculation of SST by using IR readings from two or three different spectral channels. The root mean square disagreement between calculated satellite SST and in situ ocean measurements has been shown to be 0.7°C or less. On the NOAA 6 the AVHRR has channels in the visible ($0.6 - 0.7\mu\text{m}$), near IR ($0.7 - 1.1\mu\text{m}$) and thermal IR ($3.5 - 3.9$ and $10.5 - 11.5\mu\text{m}$). These are referred to as channels 1, 2, 3, and 4, respectively. An additional channel ($11.5 - 12.5\mu\text{m}$), referred to as channel 5, is available on NOAA 7. NOAA 8, launched on March 28, 1983, has the same configuration as NOAA 6.

During a 2-day period in late November 1980, data from the NOAA 6 AVHRR were collected for a consecutive sequence of four overpasses of the Southern California Bight. During these overpasses, a large area of ocean, including the Southern California Bight, was free of clouds. Concurrently, the NOAA vessel *David Starr Jordan* was conducting a pattern of oceanographic measurements within the field of view of the NOAA 6 satellite.

Copyright 1984 by the American Geophysical Union.

Paper number 4C0574.
0148-0227/84/004C-0574\$05.00

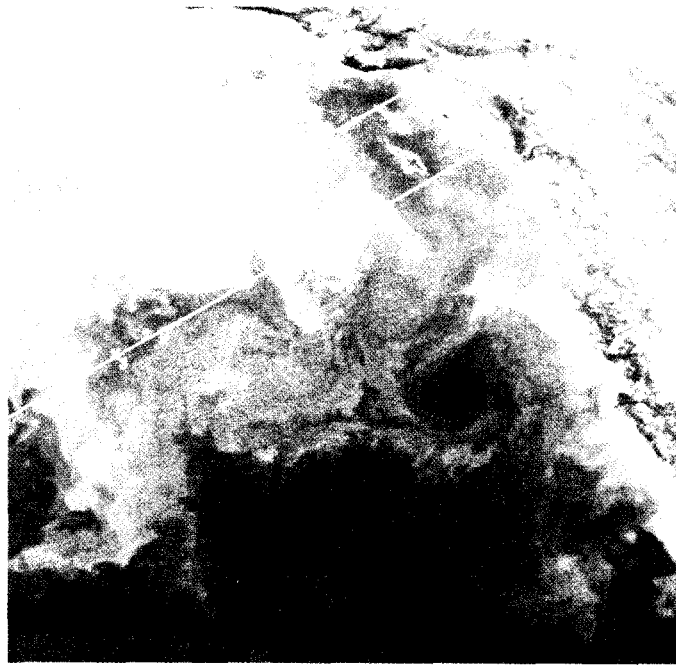


Fig. 1. Thermal image of the California Bight region made with the NOAA 6 AVHRR on November 27, 1980, at 1915 PST. Lighter shades represent lower temperatures. Different shading scales were used for land and water areas. White lines show CalCOFI transect line 86.7 (the most northern) and 90.0 sampled by R/V *Jordan* during the study. Numbered x's mark the ship's position during the sequence of satellite overpasses (discussed in text).

The clearing, which extended from inland regions to beyond 400 km offshore, was the result of a weather pattern locally termed a "Santa Ana," in which there was a broad seaward flow of low-humidity air from inland desert regions that displaced the marine cloud deck.

In this paper, multichannel atmospheric correction equations for the NOAA 6, proposed by *Bernstein* [1982] and by *McClain* [1981], are evaluated by using the satellite and in situ data set noted above. An estimate of the temporal and spatial variation of SST over small scales is made from these data, and the effect of this variation in matching satellite and in situ data sets is discussed. Additionally, changes in the temperature fields between images are examined for diurnal variation and for surface advection of horizontal temperature gradients.

Ocean Measurements

From late November through mid-December 1980 the NOAA vessel *David Starr Jordan* conducted a larval fish and oceanographic sampling survey as part of the California Cooperative Oceanic Fisheries Investigations (CalCOFI) program for the Southwest Fisheries Center/National Marine Fisheries Service. At the time of the satel-

lite overpasses the *Jordan* was occupying stations along two transects identified as lines 86.7 and 90 on the CalCOFI station grid. (The CalCOFI station grid is given in numerous publications: a recent one is CalCOFI Atlas 30 [*Lynn, et al.*, 1982], which summarizes physical oceanographic distributions.) Conductivity/temperature/depth (CTD) casts were made at stations approximately every 40 miles along line 90 by using a Plessey model 9040 CTD. The ship's tracks for these two lines and the ship positions during three of the overpasses are overplotted on the IR image for the second overpass in the series (Figure 1). (The ship position for the remaining overpass fell outside the left frame of Figure 1.) Identifying landmarks, station positions, and a geographic grid are provided in Figure 2. An Ocean Data Equipment Corporation thermosalinograph recorded surface temperature continuously. The temperature probe for the thermosalinograph is located at the intake of the sea chest, about 2 m below mean water line. The temperature channel was calibrated against high-quality reversing thermometers. The CTD casts were standardized by reversing thermometers and discrete salinity samples drawn at 1 m and at 500 m, the greatest cast depth. These casts are started with the unit submerged

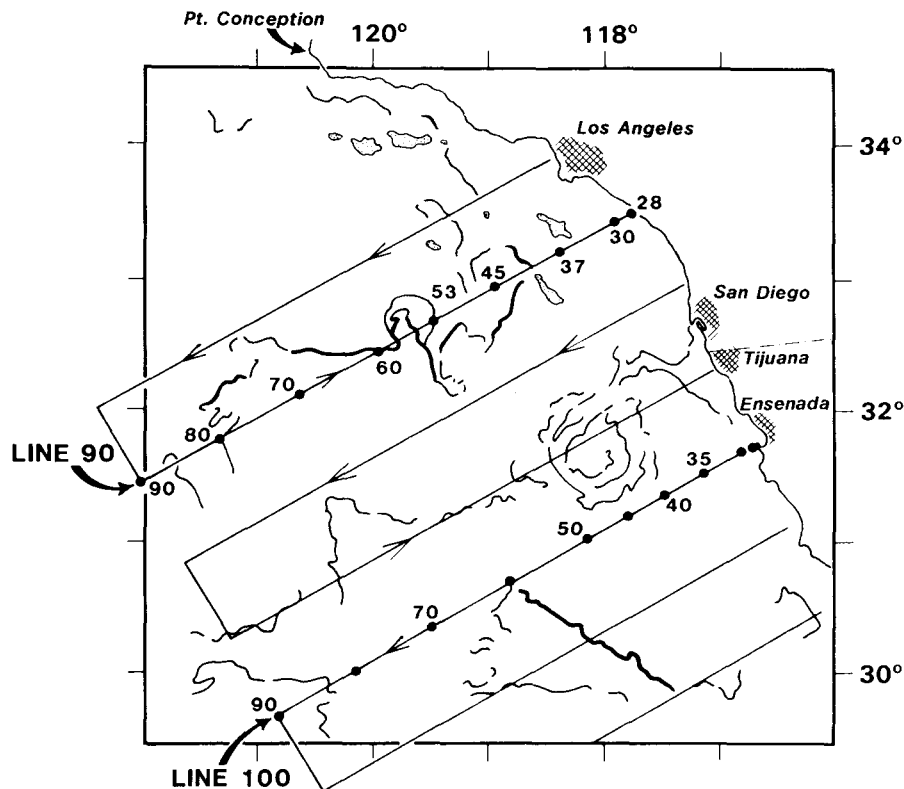


Fig. 2. Schematic of thermal patterns in Figure 1 with geographic identifications, cruise track (indicating continuous thermosalinograph recording), and CTD station positions.

and hence record temperature no shallower than 1 m. Winds and weather were recorded at CTD stations.

Satellite Measurements

The AVHRR data were collected and processed at the Scripps Satellite Oceanography Facility by using the Interactive Digital Image Manipulation System (IDIMS). The raw AVHRR signal was digitized to 10-bit resolution in equal increments of energy. Then, a radiometric calibration routine based on that of *Lauritson et al.* [1979] was used to convert the channel 3 and channel 4 energy values to units of temperature. Channel 1 and channel 2 signals were converted to percent albedo by using pre-launch constants. An orbit time correction was computed and the images were registered to an earth location accuracy of 1 pixel (1.1 x 1.1 km along subtrack) by using the method of *Young* [1981]. Image registration was checked against the location of Santa Barbara Island (33°29'N, 119°02'W). The area of this island does not greatly exceed 1 km²; hence it falls almost entirely within 1 pixel.

The first overpass was collected at 0730 PST November 27, 1980 (Julian day 332). The following three overpasses were collected at successive 12-hour intervals. These are referred to as Op 1 through Op 4, respectively; Op 1 and Op 3 are morning (descending) orbits, while Op 2 and Op 4 are evening (ascending) orbits. The subtracks of Op 1 and Op 2 fell within the bight; the subtracks of Op 3 and Op 4 fell less than 500 km to the east of it.

Description of the Study Area

Working files of full-resolution images (512 x 512 pixels) were created for analysis. Figure 1 is an image of the study area made by assigning a gray scale to channel 4 brightness temperatures of overpass 2. The image encompasses a region off southern California and northern Baja California. Point Conception is found at the upper edge of the figure and Cape Colnett, Baja California, on the lower right edge. (*Koblinsky, et al.* [1984] also used the data from these satellite passes in the study of an anticyclonic eddy and thermal fronts that lie to the north and west of the area we have framed.) Cool waters are light and warm waters are dark. The California Current transports cool waters of northerly origin southward. Inshore of the California Current, the California Countercurrent transports warmer waters of southerly origin northward (during fall and early winter). At this time the countercurrent extended northward around Point Conception as indicated by the warm (dark) coastal waters. The thermal front in the upper center of Figure 1 most probably was enhanced by the injection of cold upwelled waters into the California Current from coastal regions along central California [see *Koblinsky, et al.*, 1984]. At the thermal front the largest temperature gradient measured by the thermosalinograph is 1.7°C in 4 km. Temperatures on the cool side of the front are about 14.8°C and on the warm side 16.7°C. The warmest areas within the figure (bottom of image) are

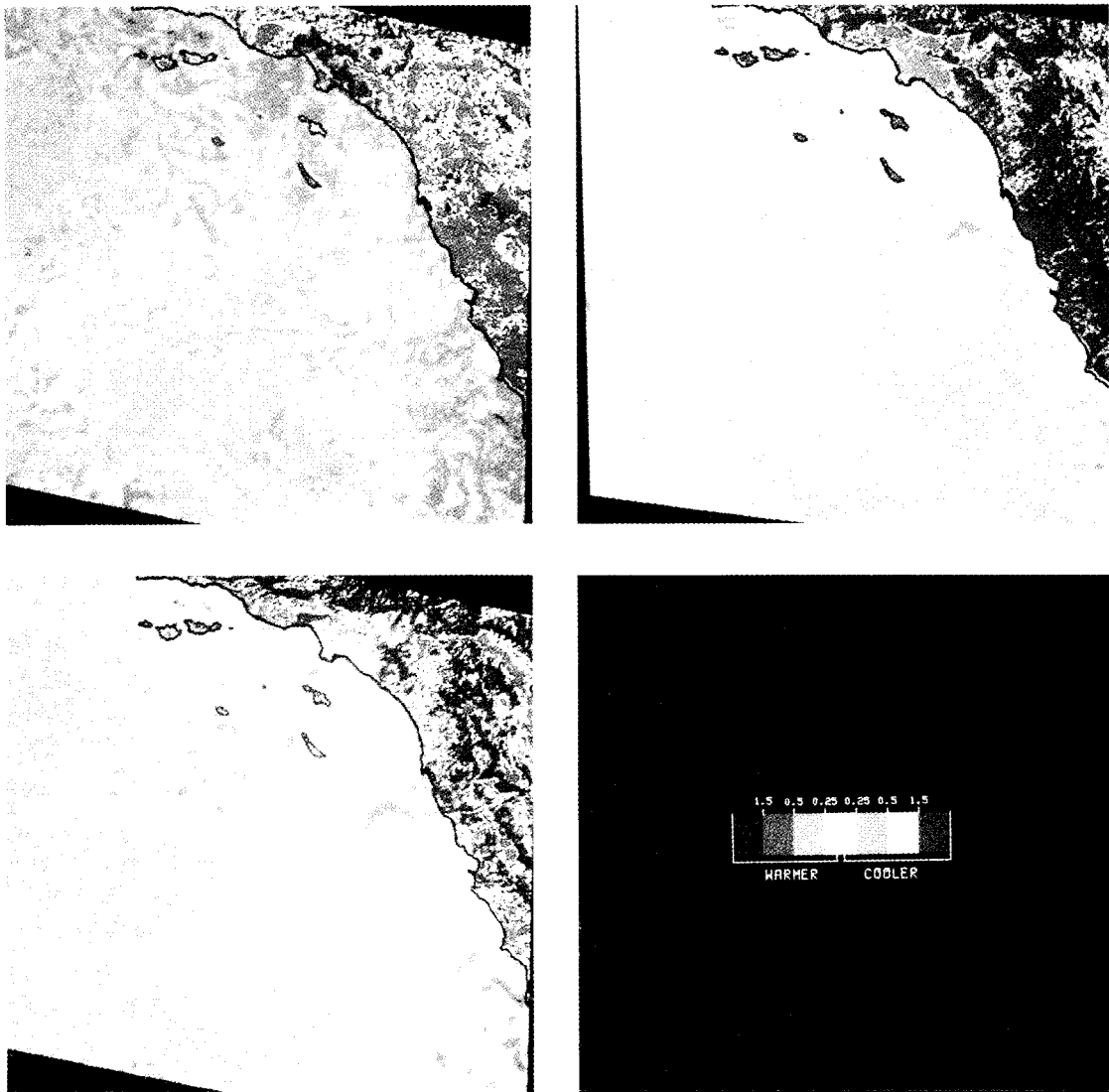


Plate 1. Differences between AVHRR channel 4 images mapped to show temperature changes during each time interval: (a) the difference between overpass 1 and 2; (b) the difference between overpasses 2 and 3; (c) the difference between overpasses 1 and 3; (d) the color key for a-c.

about 18°C. There is a cyclonic eddy west of Ensenada, Baja California, the center of which is warmer (at the surface) than the surrounding waters. The sense of eddy rotation was confirmed by surface thermal structure movement in the series of images and by geostrophic velocities calculated for stations on line 100 (Figure 2). Although the dynamics of a cyclonic eddy dictate a cool core, and the same relative pattern is expected at the surface, this eddy appears to be entraining even cooler surface waters, which have upwelled along the coast near San Diego, into its periphery.

These characteristics and features in the image of Figure 1 do not deviate appreciably from seasonal means or earlier observations. The characteristics demonstrating seasonal normality include surface temperature patterns and small pockets of coastal upwelling [*CalCOFI*, 1963; *Lynn*, 1967], flow patterns [*Wyllie*, 1966], and thermal fronts [*Bernstein et al.*, 1977]. Also, *Reid et al.* [1963] studied a cyclonic eddy in November 1959 very close to the same location as the one found in Figure 1.

THE SANTA ANA AND SUBPIXEL CLOUD DETECTION

The "Santa Ana" weather condition is characterized by winds from the midland high-desert regions, high temperatures, extremely low humidity, and complete clearing of clouds [*Sommers*, 1978, 1981]. A Santa Ana occurs when the eastern North Pacific high-pressure cell moves inland, often over northern or central California, and the inland desert low-pressure cell is situated south of it. The resulting gradient winds are directed seaward. These winds are fed by upper level dry air that descends, adiabatically warms in the eastern sector of the high-pressure cell, and is reinforced by warm dry desert air. An observer in the coastal region would note the intense blue of the sky. A Santa Ana is an infrequent occurrence in its fully developed state. It is more likely to occur in late fall and winter than at other times and typically lasts for several days. The extreme dryness associated with Santa Anas often creates serious fire hazard conditions in coastal brush and forest regions [*Sommers*, 1981]. Such conditions occurred during this study.

An important criterion for successful employment of any atmospheric correction is that the area of interest be free of clouds, including very small or transparent clouds that may remain undetected upon visual inspection of the image. The reflectance value for each pixel, as measured by channel 2, can be used to detect unresolved subpixel-sized clouds in daytime images [*Bernstein*, 1982]. A totally cloud-free atmosphere will result in an albedo of the ocean surface of less than 2% [*Bernstein*, 1982]. In our study area, no pixel showed greater than 1.7% albedo, with most pixels registering less than 1.3%. The largest albedo values were associated with a seaward projecting smoke plume originating from several brush fires. This phenomenon is discussed in a later section.

The difference between channel 3 and channel 4 and its spatial variation are also indicators of the degree of cloud contamination. This difference is used for nighttime passes when albedo measurements are not possible. The difference is usually slightly positive because of the unequal response of the two channels to water vapor.

Over very humid tropical atmospheres, it can range up to 4°C or 5°C. A much larger positive difference indicates the presence of transmissive clouds or small subresolution cloud elements, whereas a large negative difference, <-0.9°C, is indicative of thick nontransmissive clouds [*McClain et al.*, 1983]. Although this difference, theoretically, should be very close to 0 for a dry, cloudless atmosphere, the actual differences will be slightly negative (-0.1° to -0.7°C) due to molecular absorption of atmospheric gases other than water vapor (*E. P. McClain*, personal communication, 1983). Within our study area, the channel difference consistently ranged between 0.0°C and -0.6°C for all four passes. Thus both albedo values for the daytime passes and the differences between channels 3 and 4 for daytime and nighttime passes confirm the relatively dry, cloud-free conditions during our experiment. In Op 4, clouds had moved into the southwest corner of the field. Our analysis is confined to the clear areas.

SATELLITE DATA NOISE REDUCTION

From its initial operation after launch, July 1979, the channel 3 signal of the AVHRR aboard NOAA 6 has been sensitive to interferences purportedly generated by improper isolation from other circuits in the spacecraft. (Channel 3 in NOAA 7 and NOAA 8 also have had the same problem. An on-gassing procedure resulted in a 90% reduction in noise level as of June 15, 1983 (NOAA 6), September 8, 1983 (NOAA 8), and September 17, 1983 (NOAA 7) (*E. P. McClain*, personal communication, 1983).) The interference is manifested as a noise added to the sensor signal. The noise progressively increased in magnitude with time so as to make channel 3 unusable, for all practical purposes, by May 1981. In November 1980 the noise was on the order of $\pm 0.3^\circ\text{C}$, with occasional spikes to $\pm 1^\circ\text{C}$ (the effect of which is increased by 50%, using either SST correction equation). In imagery, most of this noise appears as a mottled herringbone pattern. However, all the major ocean thermal gradient features are easily discernible. The noise is susceptible to filtering because of its regularity.

The temperature signals sensed by channels 3 and 4 differ slightly because each responds differently to atmospheric gases and water vapor. Prior to filtering channel 3, the noise is enhanced in relation to the signal by creating a file of the difference between channels 3 and 4. This step removes most of the signal (i.e., the ocean temperature structure) and leaves the difference in response of the two sensors to atmospheric and the noise. Then, a two-dimensional Fast Fourier Transform (FFT) routine, available in IDIMS, is applied. The division between the remaining signal and the noise is subjectively identified on a display of the magnitude of the transform. The portions of the transform that contain the signal information are masked and an Inverse Fast Fourier Transform (IFT) is applied to the remainder (the noise), which then is subtracted from channel 3 to create a virtually noise-free channel 3 signal. The resulting image is very clean and shows the same fine-scale thermal structure as an image of channel 4. Plots of brightness temperature for channel 3, before and after filtering, and for channel 4 are given in Figure 3 for a line of pixels coincident with the ship's

track along CalCOFI line 90. Along most of this line, the filtering appreciably reduces the noise. A problem is created, however, by the filtering procedure in the daytime images within 50 km of the coast (on the right side of the plots of Figure 3, covered by shading), where the temperatures of the filtered channel 3 deviate sharply from the unfiltered data and from the form of the channel 4 plot. This is the effect of the FFT-induced smoothing across the abrupt temperature change between ocean and land. There is also a very small shadow effect, which ripples out from the coast. It is seen as ghostly repetitions of the coastline in an image formed by differencing channels 3 (filtered) and 4, and it has an amplitude of approximately 0.1°C. The problem was not evident in the night images, when the ocean/land temperature differences were small. In this study we have avoided the heavily affected areas within 50 km of the coast; the small-amplitude ripple effect was ignored. A technique that may avoid this problem, but which we have not tested, is to assign to all land areas a single value of temperature difference close to that found in coastal waters prior to applying the FFT filter.

CORRECTED SATELLITE AND IN SITU SST

The dual-channel empirical equation for calculating surface temperature (T_{sc}) from NOAA 6 data given by McClain [1981] is

$$T_{sc} = 1.5T_3 - 0.44T_4 + 1.12$$

where T_3 and T_4 are brightness temperatures for channels 3 and 4 and all temperatures are in degrees Celsius. It was developed from a simulation model by using measured atmospheric moisture and temperature profiles, and it was adjusted by linear regression to fit a set of 41 paired observations of ocean and satellite data selected for seasonal and geographic diversity. Bernstein [1982] developed an alternate version of a temperature correction equation by using only daytime passes, a rigorous screening process to obtain cloud-free satellite data, and a different set of paired ocean and satellite data. His version, after transformation and using temperatures in degrees Celsius, is

$$T_{sc} = 1.3826T_3 - 0.31T_4 + 1.72$$

The Bernstein version gives slightly higher temperatures: 0.3°C higher for $T_3 = 15^\circ\text{C}$ and $T_3 - T_4 = 4^\circ\text{C}$ (moist atmosphere) and 0.9°C higher for $T_3 = 15^\circ\text{C}$ and $T_3 - T_4 = -0.5^\circ\text{C}$ (dry atmosphere). The offset increases slightly for higher temperatures.

One of the critical steps in the algorithms of Bernstein [1982] for NOAA 6 and McClain *et al.* [1983] for NOAA 7 is the selection of those elements of a satellite image that are most likely to be free of contamination by clouds. Criteria for selection include the magnitude of the readings from various channels (to fall within specified ranges), the relationship between the readings of various channels, and the degree of variation among neighboring data elements. It is characteristic of these selection

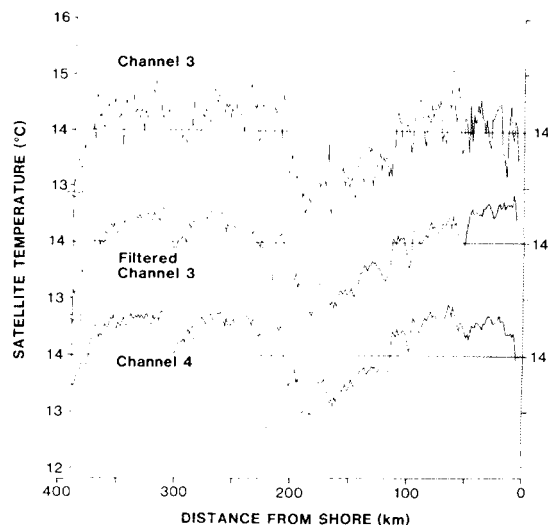


Fig. 3. NOAA 6 AVHRR temperature profiles along CalCOFI line 90 from overpass 3 (morning): top, unfiltered channel 3; middle, channel 3 after application of FFT filter; bottom, unfiltered channel 4. Lightly stippled area shows extent of land/water boundary effect in the filtered image.

processes to greatly reduce the spatial resolution. Generally, these algorithms are used to produce large-scale SST maps based on an accumulation of multiple satellite passes. Because we are examining a single area that we judge to be uniformly clear of cloud contamination, we have applied the SST correction formula to full spatial resolution of the AVHRR data without the element-by-element selection.

Estimates of sea surface temperature were computed by using both the Bernstein and McClain atmospheric correction equations. In both instances the input was channel 4 and filtered channel 3 brightness temperatures. Both versions of SST, computed for Op 3, are plotted in Figure 4 for the line of pixels corresponding to CalCOFI line 90. The thermograph trace, reconstructed to a linear distance scale, is plotted with both versions of satellite SST. This segment of the thermograph trace was recorded over 36 hours on an inbound leg of the survey pattern. The passage times of Op 3 and Op 4 are marked on the time abscissa for the thermograph.

There is excellent agreement in the spatial structure of SST between the satellite and ship records. The agreement is best where the records are more nearly coincident in time (in the neighborhood of the time of Op 3). In terms of values of temperature for this daytime overpass the Bernstein equation has a mean bias of +0.5°C in relation to the in situ measurements and the McClain equation a bias of -0.4°C. In both cases they are within the range of scatter claimed by the authors; however, they differ from each other by 0.9°C, more than their individual anticipated range of scatter. The biases attained by these simple linear models, however, are a considerable improvement over earlier versions. There is a variety of possible causes for the level of uncertainty in the models, and these causes may also be responsible for the differences between them. Both models were fitted to sets of

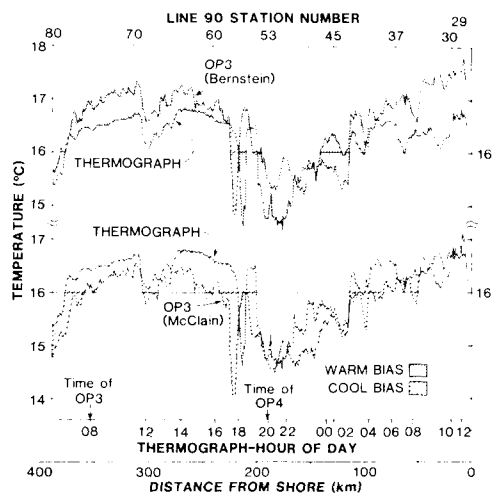


Fig. 4. Line 90 *Jordan* thermograph profile and corresponding satellite profiles using data from November 28 morning overpass (OP 3). Channel 4 and filtered channel 3 were used for Bernstein's (upper) and McClain's (lower) atmospheric correction formulae. Lightly stippled area same as Figure 3.

ocean temperature measurements (selected for quality) and corresponding satellite-derived measurements (selected as cloud-free). These paired data were collected for all seasons and for low to high latitudes. By necessity, there are tolerances in time and space needed to match ocean data to corresponding satellite data. *Bernstein* [1982] permits several tens of kilometers and several days; *McClain et al.* [1983] permits 25 km and 1 day. These tolerances contribute to the variance in deriving a satellite/ocean SST relationship. Additional problems in pairing remotely measured and in situ temperatures, noted by the authors, include using satellite areal averages versus ocean point values, diurnal variations, and true surface or "skin" values versus bulk values (usually measured at 1 or more meters below the surface). All but the last problem can be examined in our series of images.

SMALL-SCALE SPATIAL AND TEMPORAL VARIATIONS

Plots of channel 4 brightness temperatures along line 90 for OP 1 and OP 3 are plotted on a common scale in Figure 5. These transects cross a meandering thermal front three times, producing the large gradients in the center of the figure. The gradients are about 2°C in 10 km. Elsewhere in this transect there are gradients of 0.6 to 0.8°C in several tens of kilometers. The offset of one trace from the other shows the changes in 24 hours. A lateral translation (i.e., advection) of some of the gradient features has produced local temperature changes equal in value to the spatial temperature differences. The large gradient features in the center of the transect moved eastward 15 km in this period, and the gradient near 100 km from shore moved westward 20 km. The 0.8°C cooling that occurred at 300 km from shore was caused by advection transverse to this line (determined by inspection of the sequence of thermal images). The offshore two thirds of the transect shows an overall cooling on the

order of 0.3°C . These temperature differences over short distances and periods will quickly degrade a matchup of satellite and in situ measurements that are not taken within a few hours and a few kilometers of each other. Such a requirement, however, is apparently too stringent to permit a sufficient set of data pairs for establishing a regression relationship that has reasonable geographic and seasonal applicability. Thus the necessary temporal and spatial tolerances in associating ocean and satellite measurements can account for a part of the variance in the derived temperature relationship.

OCEAN SKIN TEMPERATURE

Radiometers measure the "skin" or surface temperature of the ocean, which is usually a few tenths of a degree Celsius cooler than the temperature some tens of centimeters below [Paulson and Simpson, 1981, and other references therein]. This temperature difference occurs because the vertical heat flux just below the surface is usually upward. Most of the temperature difference occurs in the upper few millimeters, where molecular processes dominate. Below this thin layer, turbulent mixing dominates and the temperature gradient is negligible [Simpson and Paulson, 1980]. The *Bernstein* [1982] and *McClain* [1981] models for correcting satellite IR brightness temperatures were empirically fitted to bulk temperatures (1 m and deeper); hence they compensate, in a rough sense, for the bias caused by the cool skin. The magnitude of the temperature difference in the upper 10 cm, however, is dependent upon wind speed and heat transfer rates. *Paulson and Simpson* [1981] find that only half the variability in the radiometric SST is accounted for by the variability in the subsurface (1 m) temperature. Based upon their experiments, the unaccountable variability is at least 0.1°C to 0.3°C . Moreover, under very low wind conditions and strong (summer) solar heating, it can be as high as 0.5° to 0.6°C . *Hasse* [1971] showed that the diurnal temperature variation within this skin layer is somewhat greater than within the rest of the diurnal layer, approximating in phase and range the overlying air temperature.

DIURNAL EFFECTS

The collection of sequential imagery from day and night NOAA 6 overpasses during this study and the high

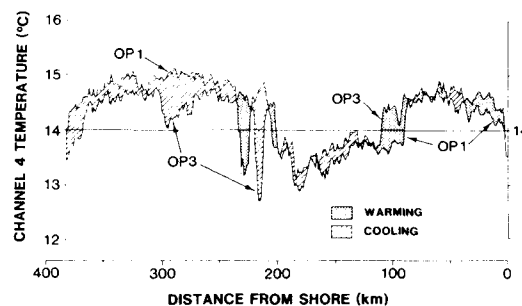


Fig. 5. AVHRR channel 4 temperatures along CalCOFI line 90 from overpasses 1 and 3 (24-hour interval).

accuracy of geographical registration of the data allowed us to examine the effects of diurnal heating as detected by the AVHRR. The formation of a shallow (less than 20 m deep) diurnal surface layer under conditions of light winds and strong insolation has been observed by numerous investigators [see, for example, *Jacobs, 1978; Kaiser, 1978*] and numerically simulated by *Dickey and Simpson [1983]*. During the day irradiative heating increases the heat content of this layer, the highest temperatures occurring in the late afternoon. The surface layer then begins to gradually lose heat during the night (or mixes the heat downward) until the temperature of the diurnal layer matches the temperature of the underlying water. A mixed layer condition persists until irradiative heating once again becomes appreciable, which is around 1000 local time for midlatitudes in autumn.

During late November, in the Southern California Bight, sunrise is at approximately 0700 and sunset at 1700 PST. The morning orbits of NOAA 6 cross the study area during the period when the diurnal layer is absent. The evening orbits pass over 3 to 4 hours after the expected peak development of a diurnal layer. The surface temperatures along line 90 are given in paired line plots by using channel 4 temperatures for each of three day/night 12-hour intervals in Figure 6. Diurnal variation in brightness temperature is clearly evident. The evening (1930 hours) temperatures are seen to be higher than the morning (0730 hours) ones by 0.2 to 0.9°C, except for small areas where shifting thermal gradients counteracted or reinforced the diurnal cycle. These differences are larger and more prevalent than the 24-hour differences of Figure 5. The differences between channels 3 and 4 remain substantially constant from Op 1 to Op 4, suggesting that the atmospheric conditions also remained constant. Therefore, the overpass-to-overpass differences in channel 4 brightness temperatures are equivalent to the differences in calculated sea surface temperatures and were chosen for examination because they are the most noise-free. These 12-hourly differences in channel 4 brightness temperatures measure diurnal heating and cooling of the oceanic thermal molecular boundary layer (the skin effect), which in turn reflects the diurnal heating and cooling of a shallow surface layer below it. The times of passage of NOAA 6 may not have caught the extremes in surface temperature, but it is not likely to have missed by much.

Maps depicting the surface temperature changes were created by subtracting thermal images, pixel by pixel, and assigning a uniform color scale to the resulting difference (Plate 1). The first of these difference maps (Plate 1a) reveals the overall diurnal warming, shown by yellow and red tones, during the period between Op 1 and Op 2 (morning to evening). The greater part of the image has a temperature increase in the range of 0.25°C to 0.5°C. Warming in excess of 0.5°C occurs south and west of Point Conception, southwest of greater Los Angeles, off Baja California, and more generally within 150 to 180 km of the coast. (Not evident in this choice of color scale is that ocean warming in excess of 1°C is confined to high gradient regions, where advection played a dominant role.) A temperature change between -0.25°C and +0.25°C occurs in the warm offshore waters (middle of Plate 1a and to the left), especially south of the leading

edge of cold water entering from the northnorthwest. There is an overall diurnal cooling in the subsequent period between Op 2 and Op 3 (evening to following morning), shown by green and blue tones (Plate 1b). The picture of cooling is roughly the reverse of the picture of warming, however, in some regions the range of diurnal cooling exceeds the warming. Most of the image has a temperature change in the range of -0.5°C to -1.5°C. (Actually the only cooling in excess of -1.0°C occurs south and west of Point Conception.) The movement of thermal gradient features over these periods produced juxtaposed patterns of strong warming and cooling in both images that mimic the features and indicate their direction of movement. For example, the cold plume extending seaward from the coast near Tijuana (Figures 1 and 2) appears in Plate 1 (especially Plate 1c) as paired warm and cold features because the plume shifted northward in the interval. The 12-hour temperature differences between Op 3 and Op 4 (not shown) are similar in pattern to Plate 1a, except that the warming was greater by nearly 0.3°C in the central and coastal portion of the image; the western and southwestern portions were contaminated by the return of offshore clouds and moisture in Op 4.

The sequence of 12-hourly SST differences shows a larger range in those waters in which the penetration of diurnal heating is constrained to a shallow layer. This includes turbid coastal areas, where the depth of penetration of solar irradiation is restricted by enhanced absorption caused by biological productivity. As a result these areas frequently have a shallow thermocline, which restricts the depth of vertical mixing. The area off Los Angeles is an example of such biologically productive waters (Plates 1a and 1b). Such observed differences in the diurnal ranges, based on variation in optical characteristics and mixed layer depth, are consistent with the results of numerical simulations by *Simpson and Dickey [1981]* and *Dickey and Simpson [1983]*. A larger range also occurs in the large plume of cool water extending southward and southeastward from near-shore regions off central California and reaching offshore of the southern Channel Islands in which infusion of coastal upwelled waters produces considerable enrichment of phytoplankton [*Simpson, 1984*]. An example of regional contrast of diurnal SST range on a much smaller scale is found in the false color images 220 km southwest of Ensenada, Baja California, where a 1°C thermal front separates a wedge of warm water to the south from cooler waters to the north (Figures 1 and 2). The warmer waters experience a wider range of diurnal change, >0.5°C, than the cooler waters, <0.5°C (Plates 1a and 1b). These observations suggest that two very different regimes of heat flux and vertical mixing might have operated on opposite sides of the front. These examples offer an interesting extension of the applicability of satellite radiometric data, and they warrant further study.

Over the encompassing 24-hour period between Op 1 and Op 3, (Plate 1), the differences are generally smaller, except for the areas affected by the movement of gradient features, most of which show larger changes. In the far offshore areas and the cooler northern waters, cooling predominates, some of which is in excess of -0.5°C. Negligible differences predominate in the central

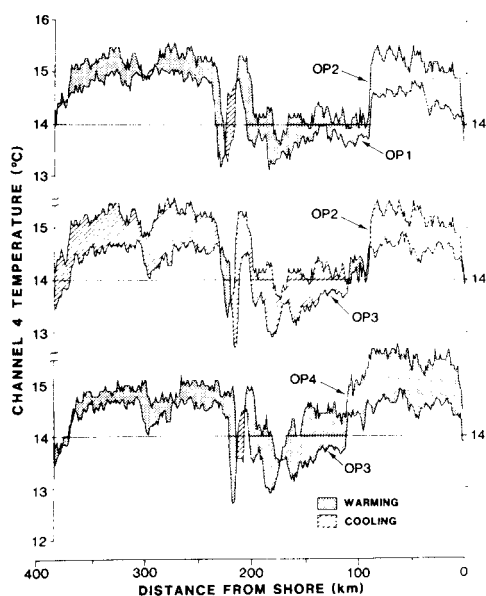


Fig. 6. AVHRR channel 4 temperature profiles along line 90, showing 12-hour differences. Shading shows extent of warming or cooling during the time interval: upper, overpass 1 (0730 hours) and overpass 2 (1930 hours); middle, overpass 2 (1930 hours) and overpass 3 (0730 hours); lower, overpass 3 (0730 hours) and overpass 4 (1930 hours).

coastal region. Moreover, the waters off Baja California, which may be remnant of earlier upwelling, show a overall small rise in temperature. The image of 24-hour temperature differences between OP 2 and OP 4 (also not shown) exhibits small temperature increases in nearshore areas, while offshore areas have negligible changes or minor cooling.

The *Jordan* CTD casts provide some small evidence of a diurnal layer. Of the 15 temperature/depth profiles, each from a different location, three were made in the late afternoon or early evening, when a warm diurnal layer would be expected to exist. Of these three, two casts show evidence of a diurnal layer. The cast at station 90.53, made at 1945 hours, shows an 11-m-thick surface layer that is 0.2°C warmer than the remaining body of the surface layer, and the cast at station 90.60, made at 1525 hours, shows a 7-m top layer that is 0.2°C warmer. The third afternoon cast, station 100.70, had no diurnal layer but was not taken until a week after this Santa Ana clearing. The CTD casts provide only marginal confirmation for the development of a diurnal layer because their scattered deployment was not entirely satisfactory for this purpose. However, at the positions of the two stations the temperature differences between OP 3 and OP 4 (from Figure 6) are in the range of 0.4 to 0.5°C. The CTD casts show only half as much diurnal variation as the satellite brightness temperatures.

DISCUSSION

The local balance of heat exchange through the sea surface can be expressed as $Q_T = Q_I + Q_L + Q_A$, where Q_I

is the incident solar irradiation input corrected for clouds and albedo, Q_L is the combined loss resulting from net back radiation and latent and sensible heat exchange, Q_A is the heat exchange caused by advection, and Q_T is the balance of the preceding terms. For a clear day at this latitude and time of year the solar irradiation (corrected for 7% albedo) is 292 cal cm⁻² d⁻¹, as calculated by Lumb [1964], or alternately 326 cal cm⁻² d⁻¹, as taken from tables adapted from Berliand by Johnson *et al.* [1965]. Psychrometric measurements taken aboard the *Jordan* formed the basis for calculations of heat loss terms. Winds, barometric pressure, air temperature, wet bulb temperature, and a bucket temperature were recorded at nine stations during the period of the Santa Ana conditions (Table 1). The measurements were taken as a matter of routine, and no precautions were taken to ensure their quality. Despite this caveat, they are adequate for estimating the surface heat budget terms. The combined heat losses were calculated for each set of measurements of the nine stations (Table 1) after the methods given in Clark *et al.* [1974]. The balance of the gain and loss terms is on the order of +100 cal cm⁻² d⁻¹. Long-term (1961-1971) mean values of Q_I and Q_L interpolated from Clark *et al.* for this region and time of year are 238 and 272 cal cm⁻² d⁻¹, respectively. Our observations show a greater gain and lesser loss, but these differences are well within the range of scatter for these terms.

A notable result of the psychrometric computations is that the relative humidity for these stations ranged from 70% to 91%, increasing with time (Table 1). Values ranging from 10% to 28% were reported for Los Angeles (*The Los Angeles Times*) and 15% to 69% for San Diego for these same days (*The San Diego Union*). The values of relative humidity calculated from the ship measurements are in apparent contradiction to the description of a dry atmosphere. It is characteristic of a Santa Ana condition, however, that following the displacement of the clouds and the cool moist marine layer by warm dry easterly winds there is immediate renewed evaporation into a thin layer of air near the surface. The evaporation cools the air and forms a stable layer in which water vapor saturation is approached [Liepper, 1948; Noonkester, 1979]. Such a shallow layer of cool moist air below the warm dry air of Santa Ana winds was also observed by Sommers [1978]. Satellite radiometers integrate the effect of atmospheric water vapor throughout the path length of observation. We have already noted that the magnitude and sign of the difference between IR brightness temperature of channels 3 and 4 describe a dry atmosphere over the ocean for the same days. An additional characteristic of IR brightness temperatures is that the thermal contrast between warm and cold water is suppressed by the water vapor content of the atmosphere; in a dry atmosphere there is no apparent loss of gradients in the data field [Huh *et al.*, 1982]. A comparison of either channel 3 or 4 brightness temperatures (Figure 3) with the thermograph data (Figure 4) shows no suppression of measured gradients, supporting the case for a dry atmosphere. Consequently, these observations show that the marine layer was very shallow indeed; the psychrometric measurements were made at a height of 4 m above the sea surface.

The heat input occurs over a period of about 9

TABLE 1. Psychrometric measurements and observations of mixed layer depth aboard the NOAA vessel *David Starr Jordan* for the period inclusive of the four satellite passes identified in the text as Op 1 through Op 4. Calculations of the combined heat loss term (Q_L) from the heat exchange balance (see text) and relative humidity appear in the right-hand columns.

Date, 1980	Time, PST	Station	Lat., N	Lon., W	Wind Speed $m\ s^{-1}$	Wind Direction, $^{\circ}T$	Pressure mbar	Air Temp., $^{\circ}C$		Bucket Temp., $^{\circ}C$	Mixed Layer Depth m*	Q_L , $cal\ cm^{-2}\ d^{-1}$	Relative Humidity, %
								Dry	Wet				
Nov. 27	0100	87.60	32°60'	120°21'	6	340	1024	16.1	13.0	14.9		237	70
Nov. 27	0557	87.70	32°39'	121°02'	7	340	1024	16.1	14.0	14.7		246	79
Nov. 27	1130	87.80	32°19'	121°43'	8	340	1025	17.8	15.8	15.7		275	81
Nov. 27	1636	87.90	31°59'	122°24'	7	0	1023.5	15.8	14.2	15.8		190	84
Nov. 27	2150	90.90	31°25'	121°59'	9	340	1023.3	16.6	15.2	17.2	23	168	86
Nov. 28	0400	90.80	31°45'	121°19'	7	330	1019.9	15.8	14.0	15.6	15 [†]	202	82
Nov. 28	0950	90.70	32°05'	120°38'	7	340	1020	17.1	15.3	16.8	50	201	83
Nov. 28	1525	90.60	32°25'	119°58'	6	330	1017	18.0	16.7	16.7	35	203	88
Nov. 28	1935	90.53	32°39'	119°29'	5	340	1017	15.3	14.4	14.8	35	179	91

* Depth where temp is $0.2^{\circ}C < SST$ exclusive of diurnal layer.

[†] This value is probably unrepresentative of the region.

hours. If the rate of loss may be considered constant over 24 hours and advective exchanges are ignored, then $230\ cal\ cm^{-2}$ are stored during daylight hours and $130\ cal\ cm^{-2}$ are lost at night. Assuming the diurnal heat gain is restricted to 7 to 11 m, as is true of the CTD casts, the diurnal increase of temperature would be on the order of $+0.25^{\circ}C$ (actually the diurnal temperature cycle is more complex, but this simple approach serves our purpose). This estimate is consistent with the CTD casts and is consistent with the diurnal modeling studies [Dickey and Simpson, 1983] for a wind speed near $7\ m\ s^{-1}$, but it is less than the observed differences of brightness temperatures. The excess heat gain of $100\ cal\ cm^{-2}$ over 24 hours is stirred throughout the surface mixed layer (Table 1), resulting in a day-to-day temperature increase of $0.04^{\circ}C$ or less. This increase is negligible. The observed IR brightness temperature differences over 24 hours (Figure 5 and Plate 1c) suggest that local advection may have played a more important role than the balance of the other heat exchange terms during this study. The equatorward flowing California Current in the offshore waters and the poleward flowing California Countercurrent nearshore [Wyllie, 1966; Lynn *et al.*, 1982] provides the correct sense of flow to produce the offshore/nearshore pattern in the 24-hour temperature differences (Plate 1c). Sections of geostrophic velocity and associated temperature (Figure 7) for lines 90 and 100 (line 100 was occupied 11 days after line 90) give evidence that equatorward advection of cooler offshore waters and poleward advection (shown hatched in Figure 7) of warmer waters might account, in part, for the differences over 24 hours. It is clear, however, that the magnitude of the day/night brightness temperature difference is not satisfactorily explained by the ocean measurements. It may be that this difference is due, in part, to a variation in magnitude of the ocean skin effect. The results of this comparison point to a need for a better understanding of the heat exchange processes in areas cleared of clouds by warm continental airflow and the effect of these circumstances on the nature of satellite-based radiometer measurements.

It is also clear that diurnal differences can have an appreciable effect on satellite SST estimations and can be

an appreciable cause of variability if data from both nighttime and daytime orbits are used during one study. If agreement between in situ and satellite measurements is sought, it is preferable to use satellite data from the orbit least affected by diurnal surface heating. For the west coast of the United States this would be the 0730 orbit of NOAA 6, the 0400 orbit of NOAA 7, and the 0800 orbit of NOAA 8.

Bernstein's atmospheric correction equation was derived from satellite data restricted to early morning passes. (The same restriction was not applied to the in situ measurements.) Applying his equation to the evening passes gives a bias of $+1.2^{\circ}C$. Such an application appears to be inappropriate. McClain's [1981] equation was also derived from morning overpasses (E.P. McClain personal communication, 1983). As applied to the evening passes, however, his equation gives a bias of $+0.4^{\circ}C$, nearly the same bias as Bernstein's equation gives for the morning overpasses. The thermograph recorded continuously and should show effects of diurnal warming at 2 m over the 36 hours it took to complete line 90. Therefore, the bias between a transect of corrected satellite temperature, a truly synoptic measurement, and the thermograph should vary between the periods in which the thermograph detected the penetration of diurnal warming and those in which it did not. A change of $0.2^{\circ}C$ in the bias of satellite and thermograph between the morning of Op 3 and the following afternoon is suggested in Figure 4. However, the complexity of the ocean's surface thermal structure and its movement make it difficult to ascertain.

Smoke — Is There an Effect Upon Temperature Estimates?

Visual imagery from channel 1 data and reflective IR imagery from channel 2 reveal large plumes of smoke from coastal forest fires, extending southward and westward over the bight. The major fires occurred a short distance inland of the beginning of line 90. Beyond the immediate region of the source, the smoke produces an increase in albedo above that in the clearest areas of 0.4 to 1.0%. The smoke occurs in large sweeping patterns that have a characteristic scale much larger than the ocean thermal patterns. If the smoke produced a detectable

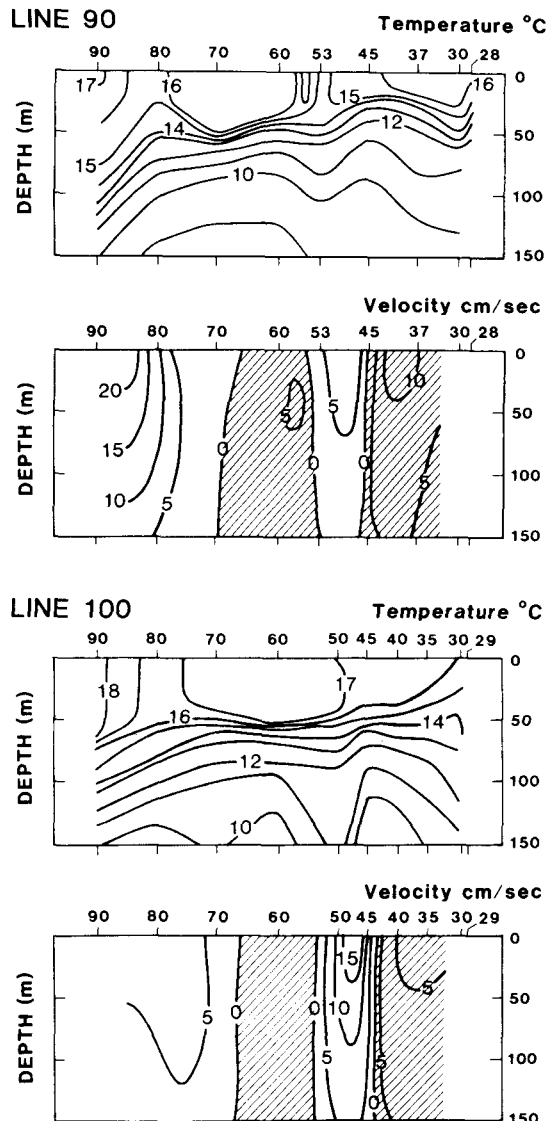


Fig. 7. Vertical sections of temperature and corresponding 0/500 db geostrophic velocity sections for lines 90 and 100. Hatching indicates poleward flow.

effect upon the IR measurements, then the smoke patterns would be found in the IR images, especially in the temperature difference between channels 3 and 4. No effect of this kind was found.

CONCLUSIONS

1. Noise in NOAA 6 channel 3 can be largely eliminated by filtering for those overpasses collected prior to spring 1981. The use of unfiltered data in estimating SST can produce spot errors as large as 1.5°C .
2. Both atmospheric correction equations tested in this case study produced estimates of SST that matched

the in situ measurements within the expected range of scatter. Bernstein's equation produced a bias (for a daytime pass) of $+0.5^{\circ}\text{C}$ and McClain's gave -0.4°C . Bernstein's version, which was derived exclusively from daytime data, produced a bias slightly in excess of 1°C when applied to nighttime data because of a diurnal variation.

3. A diurnal variation in satellite brightness temperature on the order of 0.25°C to 1.0°C was recorded in a sequence of four images. In situ measurements did not register the range in diurnal variation seen in the satellite data. This disparity is not entirely understood. There are complex heat exchange processes that occur at and near the air/sea interface (1 to $2\ \mu\text{m}$ deep) where temperature is sensed by satellite radiometers and other dynamical processes that occur at depths of 1 to 3 m, where in situ measurements of surface layer temperature are made.

4. When there is a diurnal warming of 0.3°C or more, intermixing of daytime and nighttime data will cause problems. The problems are avoided by restricting analysis to overpasses that occur at late night and early morning hours. Such a restriction should provide more reliable estimation of SST and a better match to in situ measurements. Effects of diurnal heating in in situ measurements should likewise be avoided, if possible.

5. Differences in time and/or space between satellite and in situ measurements can cause disagreements of up to 1°C or more because of surface thermal structure and its movement.

Acknowledgements. R. Michael Laurs gave his enthusiastic support for this project. Robert Bernstein and E. Paul McClain made many helpful suggestions that improved the manuscript. James J. Simpson generously provided considerable guidance in the subject of heat exchange processes as well as helpful editorial comments. This work was supported, in part, by the National Aeronautics and Space Administration, Order W15.334.

REFERENCES

- Barnett, T. P., W. C. Patzert, S. C. Webb, and B. R. Bean, Climatological usefulness of satellite determined sea-surface temperatures in the tropical Pacific, *Bull. Am. Meteorol. Soc.*, **60**, 197–205, 1979.
- Bernstein, R. L., Sea surface temperature estimation using the NOAA 6 satellite advanced very high resolution radiometer, *J. Geophys. Res.*, **87**, 9455–9465, 1982.
- Bernstein, R. L., L. Breaker, and R. Whritner, California Current eddy formation: Ship air and satellite results, *Science*, **195**, 353–359, 1977.
- CalCOFI, CalCOFI atlas of 10-meter temperatures and salinities 1949 through 1959, *CalCOFI Atlas 1*, 288 pp, Univ. Calif., San Diego, 1963.
- Clark, N. E., L. Eber, R. M. Laurs, J. A. Renner, and J. F. T. Saur, Heat exchange between ocean and atmosphere in the eastern North Pacific for 1961–71, *NOAA Tech. Rep. NMFS SSRF-682*, Nat. Oceanic Atmos. Admin., Wash., D.C., 1974.
- Dickey, T. D., and J. J. Simpson, The influence of optical water type on the diurnal response of the upper ocean, *Tellus*, **35B**, 142–154, 1983.
- Hasse, L., The sea surface temperature deviation and the heat flow at the sea-air interface, *Boundary Layer Meteorol.*, **1**, 368–379, 1971.
- Huh, O. K., L. J. Rouse, Jr., and P. F. Twitchell, Outbreaks of polar continental air: windows on the mesoscale structure of the upper ocean, *Naval Res. Reviews*, **24**, pp. 26–39, Office Naval Res., Arlington, VA, 1982.
- Jacobs, C. A., Observed oceanic variability at and near the air-sea

- interface during phase 3 of project BOMEX, *J. Phys. Oceanogr.*, **8**, 103–118, 1978.
- Johnson, J. H., G. A. Flittner, and W. M. Cline, Automatic data processing program for marine synoptic radio weather reports, *Rep. SSR-F 503*, U.S. Dep. Interior, Wash., D.C., 1965.
- Kaiser, J. A., Heat balance of the upper ocean under light winds, *J. Phys. Oceanogr.*, **8**, 1–12, 1978.
- Koblinsky, C. J., J. J. Simpson, and T. D. Dickey, An offshore eddy in the California Current System, Part 2, Surface manifestation, *Progr. Oceanogr.*, **13**, 51–69, 1984.
- Lumb, L. E., The influence of cloud on hourly amounts of total radiation at the sea surface, *Q. J. R. Meteorol. Soc.*, **90**, 43–56, 1964.
- Lauritson, L., G. G. Nelson, and R. W. Porto, Data extraction and calibration of TIROS-N/NOAA-6 radiometers, *NOAA Tech. Memo NESS 107*, pp. 44–46, U.S. Dep. Commer., Wash., D.C., 1979.
- Liepper, D., Fog development at San Diego, California, *J. Mar. Res.*, **7**, 337–346, 1948.
- Lynn, R. J., Seasonal variation of temperature and salinity at 10 meters in the California Current, *CalCOFI rep. 11*, pp. 157–186, Univ. Calif., San Diego, 1967.
- Lynn, R. J., K. A. Bliss, and L. E. Eber, Vertical and horizontal distributions of seasonal mean temperature, salinity, sigma-t, stability, dynamic height, oxygen, and oxygen saturation in the California Current, 1950–1978, *CalCOFI Atlas 30*, 513 pp., Univ. Calif., San Diego, 1982.
- Maul, G. A., and M. Sidran, Atmospheric effects on ocean surface temperature sensing from NOAA satellite scanning radiometers, *J. Geophys. Res.*, **78**, 1909–1916, 1973.
- McClain, E. P., Results of global tests of a two-window method for satellite-derived sea surface temperature, in *Applications of Existing Satellite Data to the Study of the Ocean Surface Energetics, November 1980 Workshop Proceedings*, edited by C. Gautier, pp. 169–173, University of Wisconsin Press, Madison, Wisc., 1981.
- McClain, E. P., W. G. Pichel, C. C. Walton, Z. Ahmad, and J. Sutton, Multi-channel improvements to satellite-derived global sea surface temperatures, *Adv. Space Res.*, **2** (6), 43–47, 1983.
- Noonkester, V. R., Coastal marine fog in southern California, *Mon. Weather Rev.*, **107**, 830–851, 1979.
- Paulson, C. A., and J. J. Simpson, The temperature difference across the cool skin of the ocean, *J. Geophys. Res.*, **86** (C11), 11,044–11,054, 1981.
- Reid, J. L., Jr., R. Schwartzlose, and D. M. Brown, Direct measurements of a small surface eddy off northern Baja California, *J. Mar. Res.*, **21**, 205–218, 1963.
- Simpson, J. J., An offshore eddy in the California Current System, Part 3, Chemical structure, *Progr. Oceanogr.*, **13**, 71–93, 1984.
- Simpson, J. J., and T. D. Dickey, The relationship between downward irradiance and upper ocean structure, *J. Phys. Oceanogr.*, **11**, 309–323, 1981.
- Simpson, J. J., and C. A. Paulson, Small-scale sea surface temperature structure, *J. Phys. Oceanogr.*, **10**, 399–410, 1980.
- Sommers, W. T., LMF forecast variables related to Santa Ana wind occurrences, *Mon. Weather Rev.*, **106**, 1307–1316, 1978.
- Sommers, W. T., Waves on a marine inversion undergoing mountain leeside wind shear, *J. Appl. Meteorol.*, **20**, 626–663, 1981.
- Young, T. L., User's manual for the satellite data acquisition subsystem, *Ref. 81-31*, Scripps Inst. Oceanogr., La Jolla, Calif., 1981.
- Wyllie, J. G., Geostrophic flow of the California Current at the surface and at 200 meters, *CalCOFI Atlas 4*, 288 pp., Univ. of Calif., San Diego, 1966.
- R. J. Lynn, National Marine Fisheries Service, Southwest Fisheries Center, 8604 La Jolla Shores Drive, La Jolla, CA 92038.
- J. Svejksky, Scripps Institution of Oceanography, La Jolla, CA 92093.

(Received October 17, 1983;
accepted December 16, 1983.)